Numerical analysis of attraction/repulsion collective behavior models

Francesco Vecil

Universitat de València

CISM, Udine, 12/07/2012

Outline

1. Introduction
2. Alignment model
   - Description
   - Numerical results
3. Asymptotic-speed model
   - Description
   - Numerical results

Collective behaviors

They describe situations in which a **set of individuals** organize into **macroscopically observable patterns** by **self-organization**, without the acrive role of a leader.

Figure: A fish school

Exmaples

- Fish schools
- Bird flocks
- Insect swarms
- Sheep herds
- Micro organisms
- Averaging of prices in stock exchanges
- Diffusion of languages in primitive societies

Collective behavior categories

For the sake of clarity, we divide the collective behavior models into two categories:

Alignment models

They describe the tendency animals have to modify their orientation by mimicking what the surrounding individuals do.

Figure: A bird flock

Attractive/repulsive models

They describe the tendency of social animals which want to stay together (attraction), nonetheless not too close so as to avoid collisions (repulsion).

Figure: A sheep herd

Collective behavior level of description

The collective behavior models are classified depending on the precision.

Particle (also called *individual-based*) models

Individuals are numbered from 1 to N.
Advantage: very precise, nature is discrete.
Drawback: Numerically too costly to simulate for real applications.

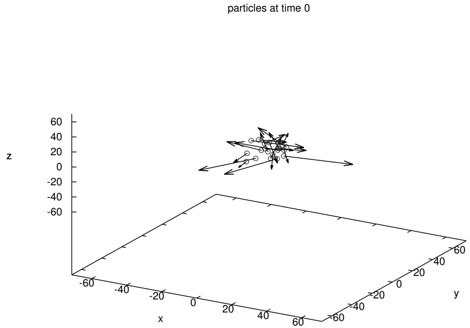

Collective behavior level of description

Continuum models

The population of individuals is described through a continuum function ρ, at different precision levels:

- In *kinetic* (or *mesoscopic*) models ρ depends on **position** and **velocity**.
  Advantage: precise, can retain details (e.g. filamentation).
  Drawback: high dimensionality too costly to solve.
- In *hydrodynamic* (or *macroscopic*) models ρ **only** depends on **position**.
  Advantage: high performances due to the low dimensionality.
  Drawback: it is the least precise possible description.

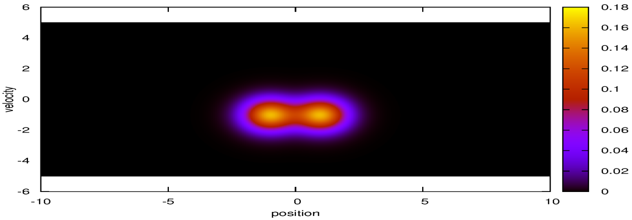

The Cucker-Smale model

Particle description

Individual number $i \in \{1, \ldots, N\}$ modifies its velocity depending on what the other individuals do:

$$\frac{d}{dt}\boldsymbol{x}^{(i)} = \boldsymbol{v}^{(i)}, \quad \frac{\mathrm{d}}{\mathrm{d}t}\boldsymbol{v}^{(i)} = -\frac{1}{N}\sum_{j=1}^{N} \frac{1}{\left(1 + |\boldsymbol{x}^{(j)} - \boldsymbol{x}^{(i)}|_{\mathbb{R}^d}^2\right)^{\gamma}} \cdot \left(\boldsymbol{v}^{(i)} - \boldsymbol{v}^{(j)}\right).$$

Known facts about this model

- For $\gamma \leq \frac{1}{2}$ the interaction is strong and the system always converges to the asymptotic state $v_i(t) \xrightarrow[t\to+\infty]{} \langle v(0)\rangle$.
- For $\gamma > \frac{1}{2}$ the interaction is weaker and the system converges to the asymptotic state $v_i(t) \xrightarrow[t\to+\infty]{} \langle v(0)\rangle$ provided that the positions and the velocities are not too *spread-out* in a certain parameter space.

The Cucker-Smale model

Cone of vision

That each bird be able to see all the surrounding birds is non-physical. Therefore, a modified version of the model is taken into account by introducing a cone of vision:

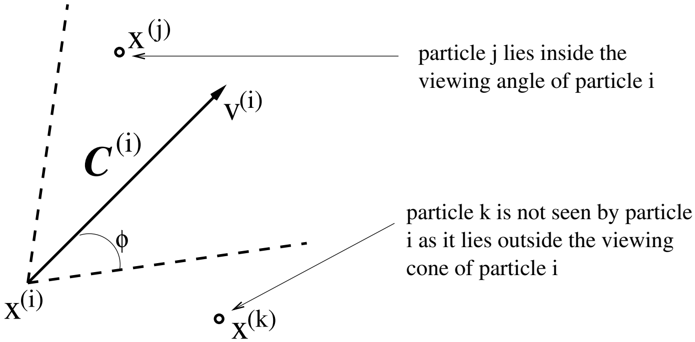

The Cucker-Smale model

Cone of vision

The original model

$$\frac{d}{dt}\boldsymbol{x}^{(i)} = \boldsymbol{v}^{(i)}, \quad \frac{\mathrm{d}}{\mathrm{d}t}\boldsymbol{v}^{(i)} = -\frac{1}{N}\sum_{j=1}^{N} \frac{1}{\left(1 + |\boldsymbol{x}^{(j)} - \boldsymbol{x}^{(i)}|_{\mathbb{R}^d}^2\right)^{\gamma}} \cdot \left(\boldsymbol{v}^{(i)} - \boldsymbol{v}^{(j)}\right).$$

is modified:

$$\frac{\mathrm{d}}{\mathrm{d}t}\boldsymbol{v}^{(i)} = -\frac{1}{N}\sum_{j=1}^{N} \frac{\mathbb{1}\left[\cos\left(\boldsymbol{x}^{(j)} - \boldsymbol{x}^{(i)}, \boldsymbol{v}^{(i)}\right) \geq \cos(\phi)\right]}{\left(1 + |\boldsymbol{x}^{(j)} - \boldsymbol{x}^{(i)}|_{\mathbb{R}^d}^2\right)^{\gamma}} \cdot \left(\boldsymbol{v}^{(i)} - \boldsymbol{v}^{(j)}\right),$$

$$\cos\left(\boldsymbol{v}', \boldsymbol{v}''\right) = \frac{\sum_{n=1}^{d} v'_n v''_n}{|\boldsymbol{v}'|_{\mathbb{R}^d} |\boldsymbol{v}''|_{\mathbb{R}^d}} \quad \text{cosine between } \boldsymbol{v}' \text{ and } \boldsymbol{v}''.$$

where ϕ is the viweing angle.

The Cucker-Smale model

Kinetic description

For $N \to \infty$ the continuum model is obtained

$$\frac{\partial f}{\partial t} + \boldsymbol{v} \cdot \boldsymbol{\nabla}_x f - \nabla_v \cdot \left[\left(\boldsymbol{v} \star_v \frac{1}{(1+|\boldsymbol{x}|^2)^\gamma} \star_x f \right) f \right] = 0.$$

Known facts about this model

- For $\gamma \leq \frac{1}{2}$ the system converges to the asymptotic state $f(t, \boldsymbol{x}, \boldsymbol{v}) \xrightarrow[t \to +\infty]{} \rho(t, \boldsymbol{x}) \delta_{\bar{\boldsymbol{v}}}(\boldsymbol{v})$.
- For $\gamma > \frac{1}{2}$??? No results known.

Cone of vision

If we wished to add a cone of vision, the system would be

$$\frac{\partial f}{\partial t} + \boldsymbol{v} \cdot \boldsymbol{\nabla}_x f - \nabla_v \cdot \left[\left(\boldsymbol{v} \star_v \frac{\mathbb{1}\left[\cos\left(\boldsymbol{x}, \boldsymbol{v}\right) \geq \cos(\phi)\right]}{(1+|\boldsymbol{x}|^2)^\gamma} \star_x f \right) f \right] = 0.$$

Outline

We shall perform a numerical analysis on three aspects:

- Leadership emergence thanks to the viewing angle.
- Convergence particle $\longrightarrow$ kinetic.
- Intuition about what happens for $\gamma > \frac{1}{2}$ in the kinetic model.

Leadership emergence

The viewing-angle structure allows for the emergence of leadership.

Viewing cone

The viewing cone of particle i is defined as

$$\mathcal{C}^{(i)} = \left\{ \boldsymbol{x} \in \mathbb{R}^d \text{such that } \left| \text{angle} \left(\boldsymbol{x} - \boldsymbol{x}^{(i)}, \boldsymbol{v}^{(i)} \right) \right| \leq \phi \right\} \subseteq \mathbb{R}^d.$$

Using graph theory to define the troops

The set of particles is a **directed graph**: an arc goes from i to j iff $P^{(j)} \in \mathcal{C}^{(i)}$. Particles i and j are *connected* iff j is reachable from i. Reachability is an equivalence relation, whose classes are called *connected components* in graph theory; we shall call them troops.

Definition of the leadership

Particle i is a leader iff $\mathcal{C}^{(i)} = \emptyset$. The number of troops and leaders evolves with time. If a troop has only one leader, then it can be inscribed inside a triangle having as vertex the leader.

Leadership emergence

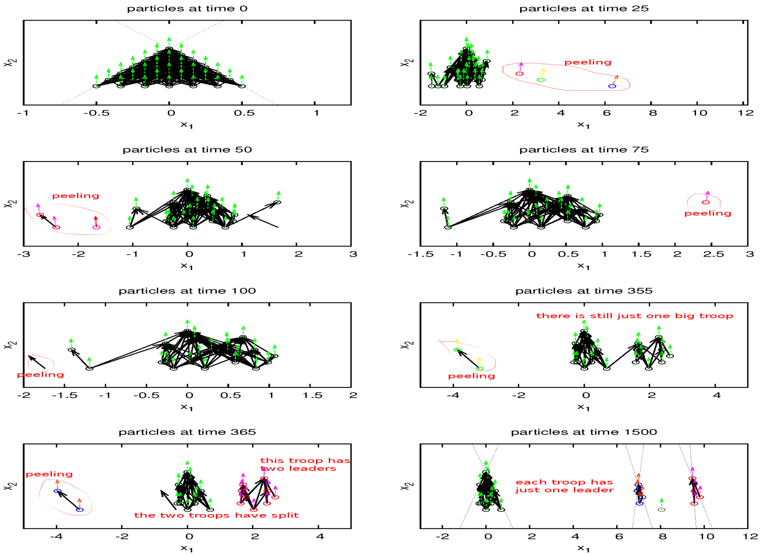

Leadership emergence

Let each troop has just one leader, let α_p the angle at the vertex, and let $\alpha := \max_{p=1,\dots,N_{\text{troops}}} \alpha_p$. Numerical evidence shows that α depends on the viewing angle ϕ.

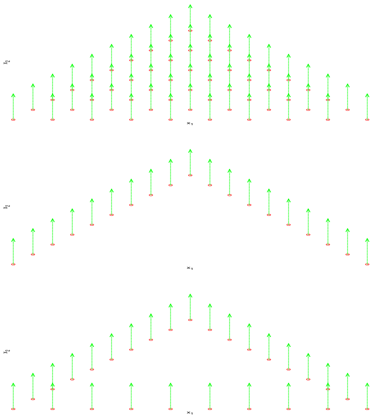

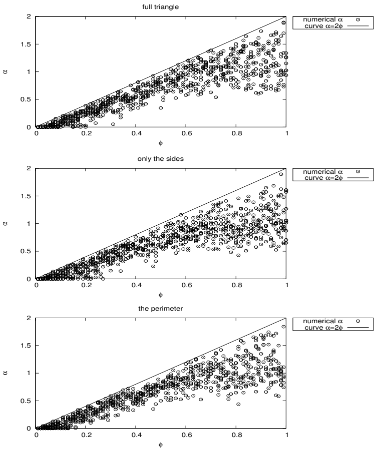

Leadership emergence: 3D case

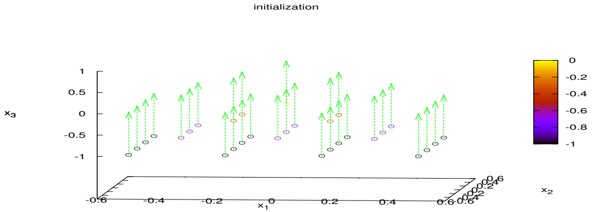

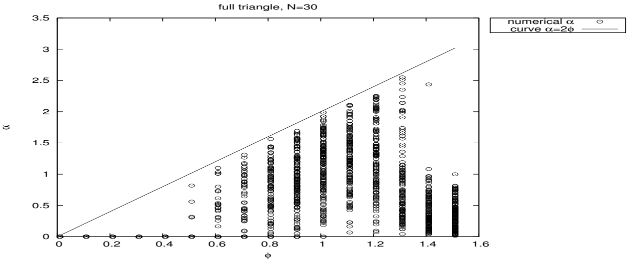

Particle/kinetic connections

Numerical scheme for the kinetic model

The kinetic code is solved through a simple WENO finite-differences scheme coupled to the TVD third-order Runge-Kutta time integrator. Just the term $\frac{\partial}{\partial v}\left[-\left(v \star_v U_0 \star_x f\right) f\right]$ requires to split the flux: let

$$a_2(x,v) := -\left(v \star_v U_0 \star_x f\right), \qquad \|a_2\|_\infty = \sup_{(x,v)} |a_2(x,v)|,$$

we rewrite it as

$$a_2(x,v) := \underbrace{\frac{a_2(x,v) + \|a_2\|_\infty}{2}}_{a_{2,+}(x,v) \geq 0} + \underbrace{\frac{a_2(x,v) - \|a_2\|_\infty}{2}}_{a_{2,-}(x,v) \leq 0}$$

so that

$$\frac{\partial}{\partial v}\left[-\left(v \star_v U_0 \star_x f\right) f\right] = \frac{\partial}{\partial v}\left[a_2(x,v) f\right] = \underbrace{\frac{\partial}{\partial v}\left[a_{2,+}(x,v) f\right]}_{\text{wind fr. left}} + \underbrace{\frac{\partial}{\partial v}\left[a_{2,-}(x,v) f\right]}_{\text{wind fr. right}}.$$

At a first glance

Numerical evidence confirms that the kinetic model is the correct limit of the particle model:

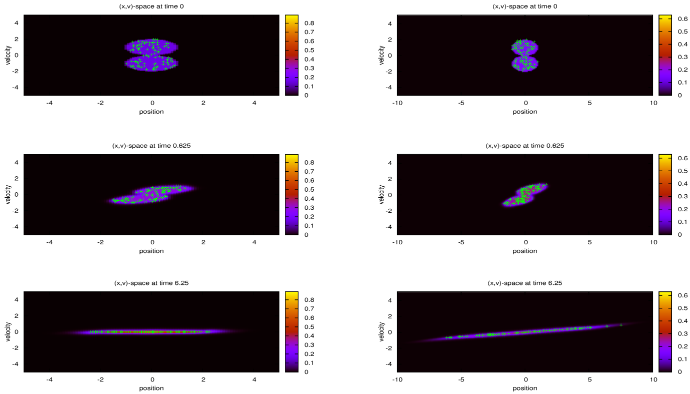

Particle/kinetic connections

Degradation rate

In the literature, it is proven that

$$W\left(\mu(t), \mu^N(t)\right) \leq C(t) W\left(\mu(0), \mu^N(0)\right),$$

where $C(t)$ has exponential growth, $W\left(\mu(t), \mu^N(t)\right)$ is the Wasserstein distance between

$$\mu(t) := \lambda\, \rho(t,x)\,, \qquad \lambda = \text{Lebesgue measure},$$

which is the particle density of the kinetic model in the sense of measures, and

$$\mu^N(t) := \frac{1}{N}\sum_{i=1}^{N} \delta\left(x - x^{(i)}(t)\right),$$

which is the particle distribution of the individual-based model.

Particle/kinetic connections

Convergence of the initial datum

We recall that $W\left(\mu(t), \mu^N(t)\right) \leq C(t)\boldsymbol{W}\left(\boldsymbol{\mu}(\mathbf{0}), \boldsymbol{\mu}^{\boldsymbol{N}}(\mathbf{0})\right)$. Let us now focus on the part concerning the initial datum (in red): numerical evidence

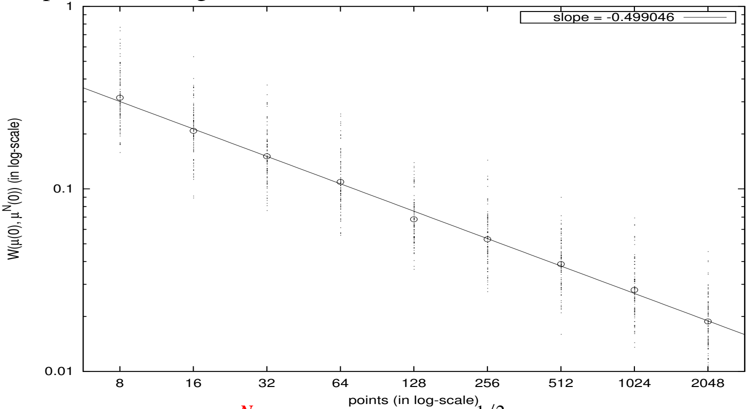

suggests that $\boldsymbol{W}(\boldsymbol{\mu}(\mathbf{0}), \boldsymbol{\mu}^{\boldsymbol{N}}(\mathbf{0})) \xrightarrow[N\to\infty]{} 0$ as $N^{-1/2}$.

Particle/kinetic connections

Exponential degradation

Again, we recall that $W\left(\mu(t), \mu^N(t)\right) \leq \boldsymbol{C(t)} W\left(\mu(0), \mu^N(0)\right)$. Empirically, $C(t)$ seems to grow at most linearly in time:

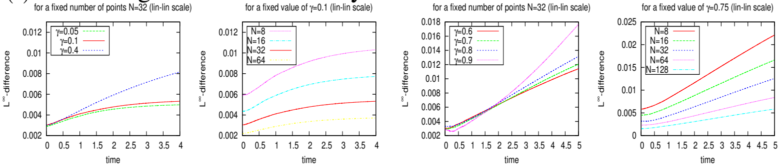

Therefore, the more optimistic $\boldsymbol{C(t)} = 1 + \mathcal{K}(\gamma)t$, might hold, with a linear dependency of $\mathcal{K}$ on the exponent γ, as suggested by numerical experiments:

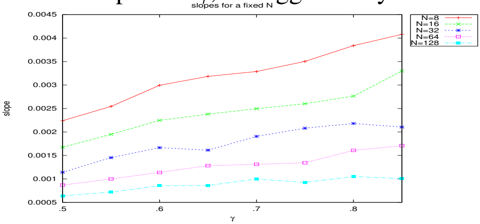

Phase transition

Relative energies

We introduce the relative kinetic and potential energies:

$$\Lambda^N := \frac{1}{2N^2} \sum_{i,j} |v^{(i)} - v^{(j)}|^2_{\mathbb{R}^d}, \qquad \Gamma^N := \frac{1}{2N^2} \sum_{i,j} |x^{(i)} - x^{(j)}|^2_{\mathbb{R}^d}.$$

In the regime $\gamma > \frac{1}{2}$, we need small values for $\Lambda^N(0)$ and $\Gamma^N(0)$ in order to ensure convergence. The phase transition from converging to diverging simulations is smooth and not sharp. Moreover, it does not seem to depend on N, which suggests similar results for the kinetic case might hold.

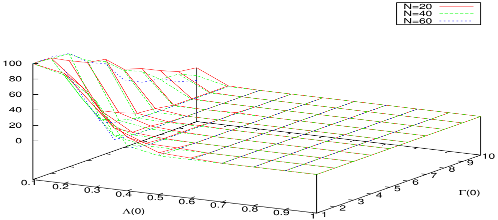

The asymptotic-speed model

We take into account three effects: selfpropulsion, friction and attraction/repulsion: for $i \in \{1, \dots, N\}$

$$\frac{\mathrm{d}}{\mathrm{d}t}\boldsymbol{x}^{(i)} = \boldsymbol{v}^{(i)}, \quad m_i \frac{\mathrm{d}}{\mathrm{d}t}\boldsymbol{v}^{(i)} = \underbrace{\underbrace{m_i \alpha \boldsymbol{v}^{(i)}}_{\text{selfpropulsion}} - \underbrace{m_i \beta |\boldsymbol{v}^{(i)}|^2_{\mathbb{R}^d} \boldsymbol{v}^{(i)}}_{\text{friction}}}_{\text{asymptotic speed}=\sqrt{\alpha/\beta}} \underbrace{- m_i \sum_{j \neq i} m_j \nabla U(\boldsymbol{x}^{(i)} - \boldsymbol{x}^{(j)})}_{\text{attraction/repulsion potential}},$$

$$U(\boldsymbol{x}) = \underbrace{-C_a \exp\left(-\frac{|\boldsymbol{x}|^p}{\ell_a^p}\right)}_{\text{attractive part}} + \underbrace{C_r \exp\left(-\frac{|\boldsymbol{x}|^p}{\ell_r^p}\right)}_{\text{repulsive part}}, \qquad p \in \{1, 2\}.$$

Kinetic model

As $N \to \infty$ we get the following kinetic model:

$$\frac{\partial f}{\partial t} + \underbrace{\boldsymbol{v} \cdot \boldsymbol{\nabla}_{\boldsymbol{x}} f}_{\text{free motion}} + \underbrace{\nabla_{\boldsymbol{v}} \cdot \left[(\alpha - \beta |\boldsymbol{v}|^2_{\mathbb{R}^d}) \boldsymbol{v} f\right]}_{\text{asymptotic speed}} - \underbrace{\nabla_{\boldsymbol{v}} \cdot \left[(\boldsymbol{\nabla}_{\boldsymbol{x}} U * \rho) f\right]}_{\text{attraction/repulsion}} = 0.$$

The asymptotic-speed model

To make the **characteristic times** appear, we adimensonalize the system:

$$\frac{d\boldsymbol{x}^{(i)}}{dt} = \underbrace{\frac{t_*}{t_{\mathrm{kin}}}\boldsymbol{v}^{(i)}}_{\text{free motion}}, \quad \frac{d\boldsymbol{v}^{(i)}}{dt} = \underbrace{\frac{t_*}{t_{\mathrm{f/p}}}(1-|\boldsymbol{v}^{(i)}|^2)\boldsymbol{v}^{(i)}}_{\text{asymptotic speed}} - \underbrace{\frac{t_*}{t_{\mathrm{a/r}}}\frac{1}{N}\sum_{j\neq i}\boldsymbol{\nabla}_{\boldsymbol{x}}\left[-W(\boldsymbol{x})+CW(\boldsymbol{x}/\ell)\right]}_{\text{Morse potential}},$$

$$t_{\mathrm{kin}} = \ell_a\sqrt{\frac{\beta}{\alpha}}, \qquad t_{\mathrm{f/p}} = \frac{1}{\alpha}, \qquad t_{\mathrm{a/r}} = \frac{\ell_a}{C_a M}\sqrt{\frac{\alpha}{\beta}}.$$

We expect that the smallest characteristic times be the first effect to appear, while the largest should indicate the asymptotic state.

Stability diagram

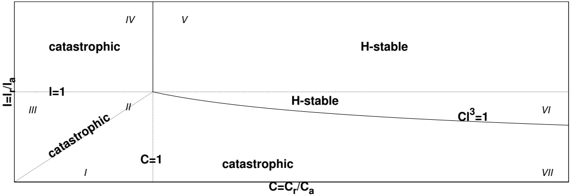

Numerical experiments

3D clumps

particles at time 80

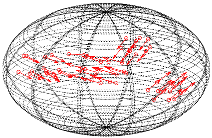

Time hierarchy is: $t_{\mathrm{a/r}} < t_{\mathrm{kin}} < t_{\mathrm{f/p}}$.

We are in region I (catastrophic): $C = .6, \ell = .5$.

trajectory of particle nr. 0 since time 80

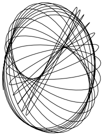

trajectory of particle nr. 1 since time 80

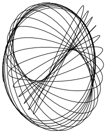

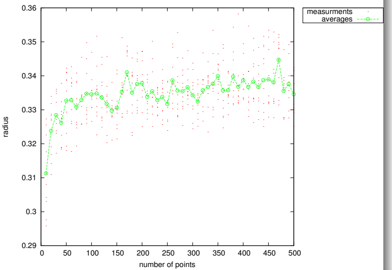

Numerical experiments

3D rings

Regions II ($C = .5, \ell = .5$), III ($C = .4, \ell = .6$) and IV ($C = .5, \ell = 1.2$) are catastrophic. Time hierarchy is: $t_{\mathrm{a/r}} < t_{\mathrm{kin}} < t_{\mathrm{f/p}}$.

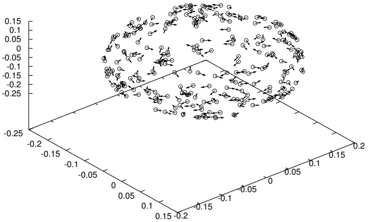

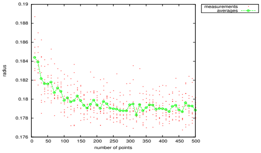

(j) (II)

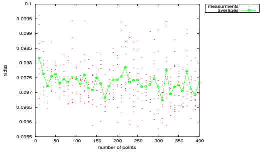

(k) (III)

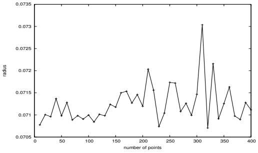

(l) (IV)

Numerical experiments

3D coherent flocks

In regions VI (stable) for small values of $\sqrt{\alpha/\beta}$ **coherent flocks** might appear, with two peculiarities: particles try to form a **crystal structure** and the coherent flock is mixed to a **rigid-body rotation**. Time hierarchy is: $t_{\mathrm{a/r}} < t_{\mathrm{kin}} < t_{\mathrm{f/p}}$.

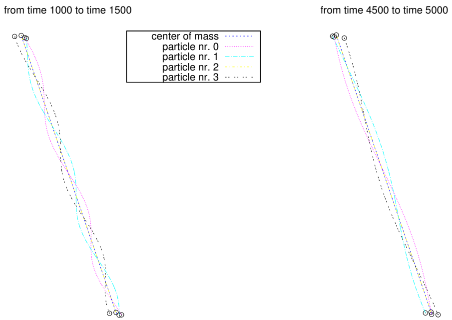

Numerical experiments

3D coherent flocks

The H-stability reflects in the increase of the radius with respect to the number of particles.
Both the increases of N and α seem to favor dispersed states.

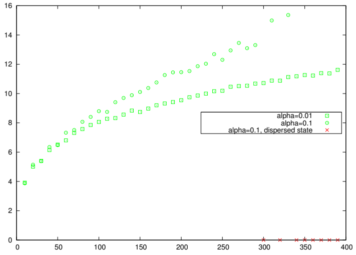

(m) radius

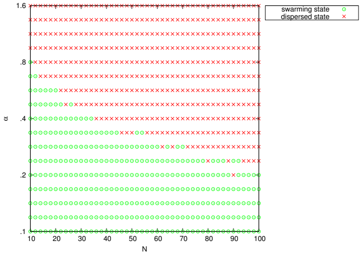

(n) α_{escape}

Numerical experiments

Some bizarre patterns...

For small numbers of particles, some bizarre patterns might emerge.

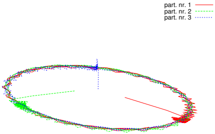

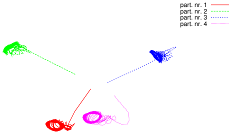

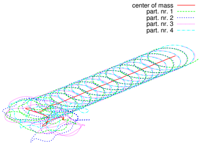

Numerical experiments

3D mills

Mills and **rigid-body** rotations are two *rotational states*. In mills, the particles keep the modulus of the velocities fixed, while in rigid-body rotations they keep fixed distances. In region VII, these two patterns might appear as stages of the same simulation.

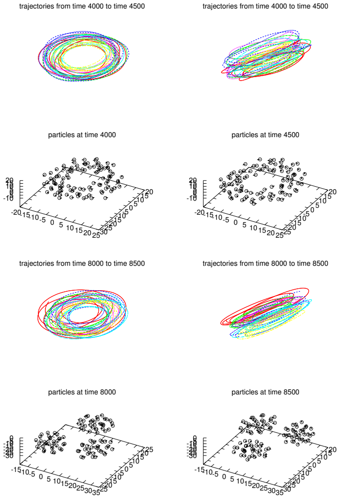

Numerical experiments

Instability of the 3D mills

Let $P := \frac{\left|\sum_{i=1}^N \boldsymbol{v}^{(i)}\right|}{\sum_{i=1}^N \left|\boldsymbol{v}^{(i)}\right|}$ (polarity), $\quad M := \frac{\left|\sum_{i=1}^N \boldsymbol{r}^{(i)} \wedge \boldsymbol{v}^{(i)}\right|}{\sum_{i=1}^N \left|\boldsymbol{x}^{(i)} - \boldsymbol{x}_{CM}\right| \left|\boldsymbol{v}^{(i)}\right|}$ (mom.).

A coherent flock corresponds to $(P, M) = (1, 0)$; a mill to $(P, M) = (0, 1)$. Numerical evidence suggests that mills are unstable: they eventually degenerate into a coherent flock. Contextually, the relative energies drop.

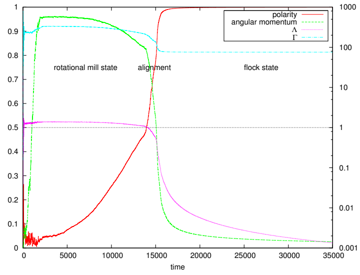

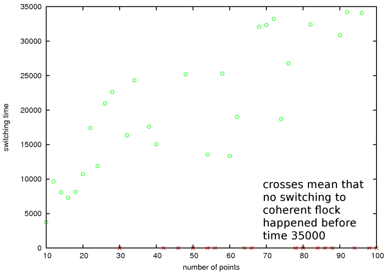

Numerical experiments

Shape of the crystal lattice

In order to study the shape of the lattice, we introduce an order factor:

$$O_Q = \frac{1}{N\binom{\mu}{2}} \left| \sum_{i=0}^{N-1} \sum_{j_1=1}^{\mu} \sum_{j_2=j_1+1}^{\mu} \cos\left(Q \cdot \phi^{(i)}_{\mathcal{N}^{(i)}_{j_1},\mathcal{N}^{(i)}_{j_2}} \right) \right|,$$

$\phi^{(i)}_{\ell,m}$ is angle $P^{(\ell)}\widehat{P^{(i)}}P^{(m)}$ and dist $\left(x^{(i)}, x^{\mathcal{N}^{(i)}_1}\right) \leq$ dist $\left(x^{(i)}, x^{\mathcal{N}^{(i)}_2}\right) \leq \dots$

O_Q is peaked at value 2 for any choice of μ $\implies$ **cubic lattice.**

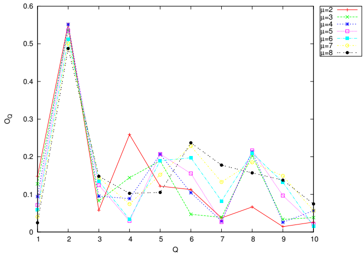

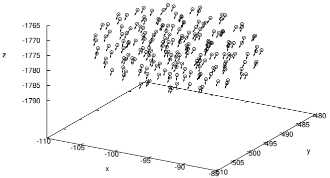

Numerical experiments

Continuum model

We perform simulations on a simplified geometry: particles turn on a circle.

Sketch of the numerical scheme

We Strang-split the solution of the PDE and solve each part for separate:

$$\partial_t f + \underbrace{\frac{t_*}{t_{kin}} v \cdot \partial_x f}_{\text{upwinding}} + \underbrace{\frac{t_*}{t_{f/p}} \partial_v \left[(1 - v^2) v f \right]}_{\text{PFC3 (conservative)}}$$
$$\underbrace{- \frac{t_*}{t_{a/r}} \partial_v \left[\left(\partial_x \left(-e^{-|x|^p} + C e^{-\frac{|x|^p}{\ell^p}} \right) * \rho \right) f \right]}_{\text{upwinding}} = 0.$$

The convolution term is computed thanks to Laguerre polynomials.

Numerical experiments

The effect of the asymptotic-speed part

The continuum simulations correctly reproduce the fact that the selfpropulsion and friction parts force the velocity to have modulus $\sqrt{\alpha/\beta}$.

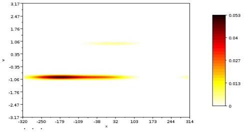

(a) Case MKR-I

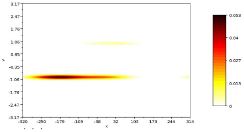

(b) Case MKR-II

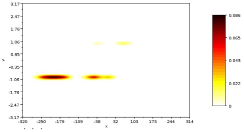

(c) Case MKR-VI-1

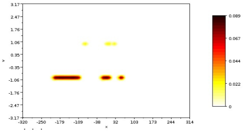

(d) Case MRK-VII-2

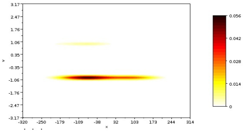

(e) Case KMR-VII

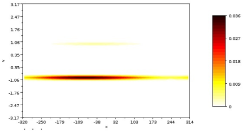

(f) Case KRM-VII

Numerical experiments

The effect of the asymptotic-speed part

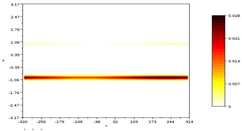

(a) Case MKR-I

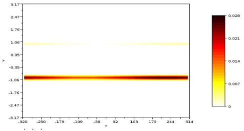

(b) Case MKR-II

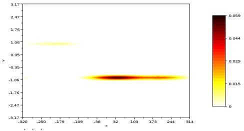

(c) Case MKR-VI-1

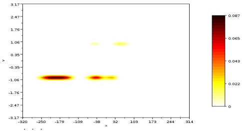

(d) Case MRK-VII-2

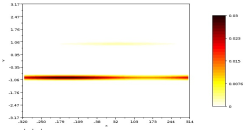

(e) Case KMR-VII

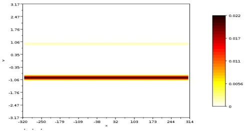

(f) Case KRM-VII

Numerical experiments

Torus view

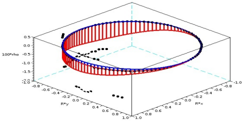

(a) Case MKR-I

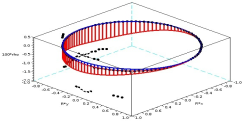

(b) Case MKR-II

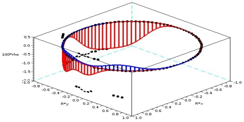

(c) Case MKR-VI-1

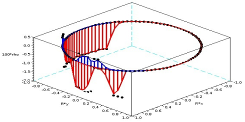

(d) Case MRK-VII-2

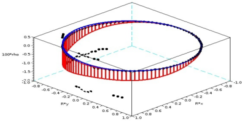

(e) Case KMR-VII

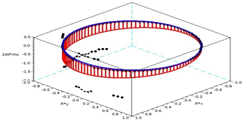

(f) Case KRM-VII

Numerical experiments

Torus view

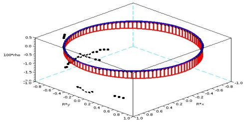

(a) Case MKR-I

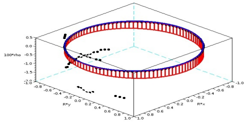

(b) Case MKR-II

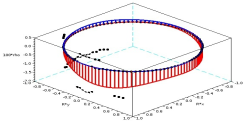

(c) Case MKR-VI-1

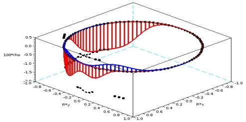

(d) Case MRK-VII-2

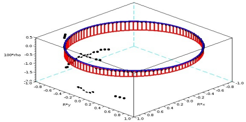

(e) Case KMR-VII

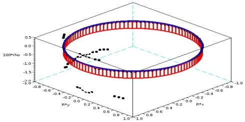

(f) Case KRM-VII

Thank you for your attention!